frontiers | Frontiers in Electronic Materials

ORIGINAL RESEARCH
published: 25 May 2022
doi: 10.3389/femat.2022.904405

Significantly Improved Energy Storage Density of Polypropylene Nanocomposites *via* Macroscopic and Mesoscopic Structure Designs

Minzun Ji[1], *Daomin Min*[1]*, *Qingzhou Wu*[2], *Rui Mi*[1], *Wenfeng Liu*[1]*, *Shengtao Li*[1], *Shaorui Qin*[3] *and Shenglong Zhu*[3]

[1]State Key Laboratory of Electrical Insulation and Power Equipment, Xi'an Jiaotong University, Xi'an, China, [2]Institute of Fluid Physics, China Academy of Engineering Physics, Mianyang, China, [3]State Grid AnHui Electric Power Research Institute, Hefei, China

OPEN ACCESS

Edited by:
Jun-Wei Zha,
University of Science and Technology Beijing, China

Reviewed by:
Qingguo Chi,
Harbin University of Science and Technology, China
Sheng Chen,
Xiangtan University, China

***Correspondence:**
Daomin Min
forrestmin@xjtu.edu.cn
Wenfeng Liu
liuwenfeng@xjtu.edu.cn

Specialty section:
This article was submitted to Dielectric Materials, a section of the journal Frontiers in Electronic Materials

Received: *25 March 2022*
Accepted: *19 April 2022*
Published: *25 May 2022*

Citation:
Ji M, Min D, Wu Q, Mi R, Liu W, Li S, Qin S and Zhu S (2022) Significantly Improved Energy Storage Density of Polypropylene Nanocomposites via Macroscopic and Mesoscopic Structure Designs. Front. Electron. Mater. 2:904405. doi: 10.3389/femat.2022.904405

Polymer dielectrics with high breakdown strength are very competitively used in the dielectric capacitor, which is widely applied in pulsed power devices and power systems due to their ultra-high power density. The polypropylene (PP) film is the most popularly used polymer for the dielectric capacitor in the market. However, its low energy density cannot meet the emerging demand for miniaturized, compact, and high-energy performance dielectrics. Therefore, it is urgent to raise the energy storage density of the polypropylene film. Here, this study described the improved energy storage density of polypropylene nanocomposites *via* macroscopic and mesoscopic structure designs. The ABA-structured, BAB-structured, and single-layered nanocomposites were prepared by melting blending and hot-pressing methods, where "A" and "B" films refer to PP/MgO and PP/$BaTO_3$ nanocomposite dielectrics, respectively. Then, the microstructure, dielectric, breakdown, and energy storage properties of these nanocomposite dielectrics were tested. According to the test results, for the sandwich-structured dielectrics, the B layer and the interface between adjacent layers can increase the polarization, and the A layer and the barrier at the interface can reduce the charge mobility. In addition, the sandwich structures can redistribute the electric field. Correspondingly, the breakdown strength and permittivity of PP dielectrics are improved synergistically. Compared to the PP nanocomposite dielectrics with the BAB structure, the dielectric with the ABA structure exhibits more excellent energy storage performance. The largest energy storage density of ABA films with a $BaTO_3$ content of 45 wt% in the B layer is 3.10 J/cm^3, which is 67% higher than that of pure PP. The study provides a new concept for improving the energy storage performance of polymer nanocomposite dielectrics from the perspective of macroscopic and mesoscopic structure designs.

Keywords: polypropylene nanocomposite, energy storage, sandwich structure, breakdown strength, dielectric properties

1 INTRODUCTION

Dielectric capacitors are capable of ultra-high power density and excellent charge-discharge stability, which can store energy by polarization mechanisms and convert the stored direct current to alternating currents and are widely used in pulse power systems, sustainable energy products such as hybrid electric vehicles, and other advanced electronics and electric power systems (Dang et al., 2013; Prateek et al., 2016; Li et al., 2018; Zhou and Wang, 2020). Polymer dielectric materials are more attractively used in capacitors because of their high breakdown strength, flexibility, lightweight, and easy manufacturing capability (Zhang et al., 2018a; Luo et al., 2019). The stored energy density U_e of dielectrics in capacitors is given as follows:

$$U_e = \int EdD, \tag{1}$$

where E is the applied electric field, and D is the electrical displacement. For the linear dielectrics, whose electric polarization is linear with the electric field, the stored energy density can be expressed as follows:

$$U_e = \frac{1}{2}\varepsilon_r\varepsilon_0 E^2, \tag{2}$$

where ε_r is the relative permittivity, and ε_0 is the vacuum permittivity (8.85×10^{-12} Fm^{-1}). Polypropylene is the most common linear dielectric used in capacitors by virtue of its high breakdown strength, low production cost, and excellent self-healing performance. The commercial biaxially oriented polypropylene (BOPP) capacitor exhibits high charge-discharge efficiency η that is larger than 90% until breakdown occurs at room temperature. However, the energy density of the BOPP capacitor is limited to around 2 Jcm^{-3} (Ho et al., 2007; Luo et al., 2019; Ru et al., 2021). To meet the emerging demand for miniaturized, compact, and high-energy performance capacitors, it is urgent to raise the energy storage density of dielectric capacitors (Chen et al., 2015). From the energy density formula of linear dielectrics, it can be seen that increasing relative permittivity and breakdown strength can elevate the storage energy density of dielectrics.

On one hand, some efforts have been made to improve the energy density by increasing relative permittivity. Mixing the conductive filler and inorganic nanofillers with high polarization characteristics into the polymer dielectrics, such as Ag (Zhang et al., 2016), graphene oxide (Fang et al., 2015; Zhi et al., 2015), $BaTiO_3$ (BT) (Dang et al., 2008; Niu et al., 2018), $SrTiO_3$ (Liu and Zhai, 2015), and $Ba_{0.2}Sr_{0.8}TiO_3$ (Tang and Sodano, 2013) nanoparticles, can significantly increase the relative permittivity of the dielectrics. However, the large increase in relative permittivity at the expense of the breakdown strength causes an increase in the dielectric loss, which reduces the charge-discharge efficiency (Yu et al., 2013). On the other hand, some works focused on improving the energy density by increasing the breakdown strength (Li et al., 2019; Zhu et al., 2019). Low-κ inorganic fillers with a broad band-gap play an important role in enhancing the electrical insulation performance of polymer nanocomposites (Thakur et al., 2017; Ai et al., 2020; Ren et al., 2021). Liu et al. prepared a ternary composite by mixing montmorillonite (oMMT) and boron nitride (BN) into the PP matrix. The breakdown strength of the PP/oMMT/BN ternary composite is 22.9% higher than that of pure PP (Liu et al., 2019). In addition, increasing work has been devoted to synergistically improving the permittivity and breakdown field strength (Zheng et al., 2018; Zhou et al., 2020). Mixing the nanofillers with high breakdown strength and nanofillers with a high dielectric constant in the polymer matrix is also an effective method to enhance the energy storage performance of dielectrics. On the basis of the addition of various nanofillers, the multilayer structures and gradient structures can be constructed by further optimizing the distribution of nanofillers in the polymeric matrix, which can synergistically improve the dielectric and breakdown performance to a greater extent (Zhang et al., 2018b; Jiang et al., 2019; Wang et al., 2022). The multilayer structures can modulate the constitute and physical properties of every layer to further optimize the electric field distribution and also can build a barrier between layers to reduce the carrier mobility, leading to a comprehensive improvement of energy storage performance. At present, the effect of multilayer structures on energy storage performance for some polymer materials, such as polyvinylidene difluoride, polyimide dielectrics, poly (methyl methacrylate), has been studied (Wang et al., 2015; Liu et al., 2017; Wang et al., 2017; Marwat et al., 2019; Li et al., 2020; Ru et al., 2021). However, there is rare research on multilayer structures of PP dielectrics for storing energy.

In this work, the single-layered and sandwich-structured PP nanocomposite dielectrics were prepared by melt blending and hot-pressing. The PP/MgO nanocomposite layer with an MgO content of 0.5 wt% was employed as a high breakdown layer and PP/BT nanocomposite layers as high polarization layers. It shows that the energy density of sandwich structures with a high breakdown layer as outer layers and a high polarization layer as the middle layer is the largest, which is 67% higher than that of pure PP while maintaining good energy storage efficiency. The study provides a new concept for optimizing electric field distribution, reducing the surge of strong field conductivity, and improving the energy storage performance of polymer nanocomposite dielectrics from the perspective of macro- and mesoscopic structure designs.

2 MATERIALS AND METHODS

2.1 Materials and Preparation

Polypropylene (HC312BF, pellets) was purchased from Borealis. MgO (50 nm in diameter) and $BaTiO_3$ (90 nm in diameter) nanoparticles were purchased from Deke Daojin Science and Technology Co., Ltd. The polypropylene nanocomposite films were fabricated through melt blending and hot-pressing. A two-step method was used in the melt blending process. First, a PP-based blend with a high concentration of nanoparticles was prepared as a masterbatch. Second, an appropriate amount of polypropylene pellets used as the "diluter" was blended with the

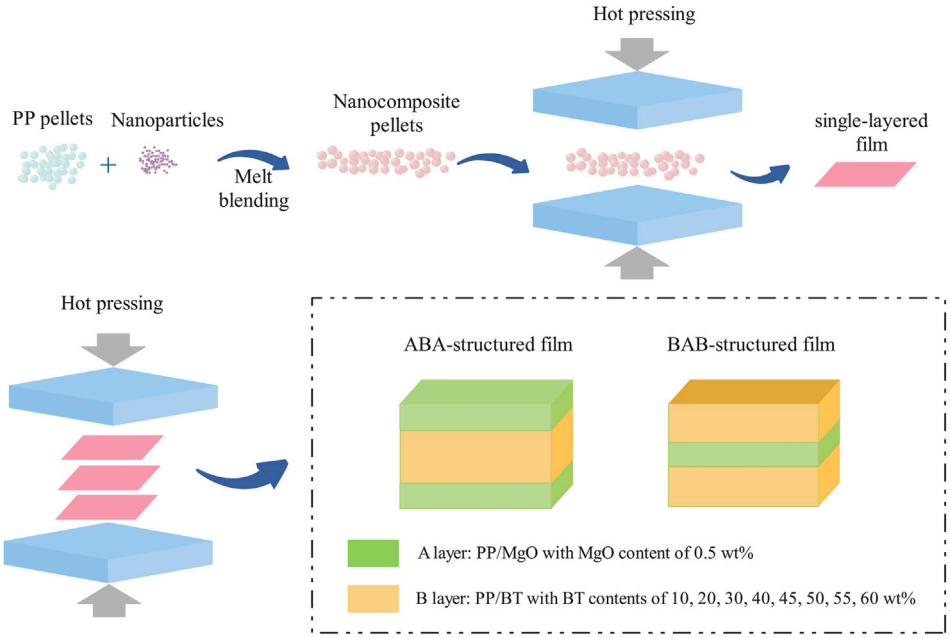

FIGURE 1 | Schematic diagram of sample preparation.

masterbatch to obtain a product with a target concentration of nanoparticles.

2.1.1 Preparation of Single-Layered PP/BT and PP/MgO Films

First, PP pellets were added to a torque rheometer (RM-200C, Harbin Harp Electrical Technology Co., Ltd, China) and melted at the setting temperature of 180°C and a rotation speed of 50 r/min. After the PP pellets were completely melted, the nanoparticles were added to the torque rheometer. Then, the masterbatch with a high concentration of nanoparticles was prepared. Second, an appropriate amount of polypropylene pellets were blended with the masterbatch to obtain nanocomposites with the target concentration. Third, the hot press process was conducted by using a plate vulcanizing press machine. The weighed nanocomposite blend was put into a mold. The mold with the blend was preheated under no pressure for 20 min on the plate vulcanizing press. Then, a step-by-step method was used to increase the pressure on the exhaust. In other words, the mold was pressed under 5 MPa for 5 min, then pressed under 10 MPa for 5 min, and finally pressed under 15 MPa for 5 min. Keeping pressure and water-cooling to about 35°C, the single-layered film was obtained by removing the mold. The PP/MgO nanocomposite film with the MgO content of 0.5 wt% is denoted as "A", which has a high breakdown strength and was used as an insulation layer. The PP/BT nanocomposite films with BT contents of 10, 20, 30, 40, 45, 50, 55, and 60 wt% were denoted as "B-x" (x wt% of the BT content), which have high relative permittivity and are regarded as polarization layers. The single-layered A with a thickness of 25 μm and 100 μm and B with a thickness of 37.5, 50, and 100 μm were prepared.

2.1.2 Preparation of Sandwich-Structured ABA and BAB Films

There are two kinds of sandwich-structured films: "ABA" and "BAB". 1) 25-μm-thick A and 50-μm-thick B were stacked together in the order of A-B-A in the mold. Under the pressure of 10 MPa, the mold with layers was hot-pressed at 170°C for 5 min 2) Two 37.5-μm-thick B layers with the same content of BT and one 25-μm-thick A layer were stacked together in the order of B-A-B in the mold. The hot-pressing process was the same as that of ABA. The sandwich-structured ABA and BAB with a thickness of about 100 μm were prepared. For further differentiation, the sandwich-structured films were abbreviated as "ABA-x" or "BAB-x" (x wt% of BT content in the B layers).

The single-layered A and B with a thickness of 100 μm were used as the controls. The whole sample preparation is shown in **Figure 1**.

2.2 Characterization

The cross-sectional morphologies of single-layered and sandwich-structured films were characterized by scanning electron microscopy (SEM, GeminiSEM 500, Zeiss, Germany). The mass crystallinity of the films was obtained by a differential scanning calorimeter (DSC, DSC822e, METTLER TOLEDO, Switzerland). Under the nitrogen atmosphere, the DSC tests were conducted on the sample with a mass of 7 ± 0.5 mg from 30 to 250°C with a heating rate of 10°C/min. The equation for calculating the mass crystallinity X_{DSC} is as follows, $X_{DSC} = \Delta H/\Delta H_0$, where ΔH is the melting enthalpy of DSC curves, J/g; ΔH_0 is the melting enthalpy of PP with the crystallinity of 100% (240.5 J/g). The grain size of the films was tested by X-ray diffraction (XRD, D8 ADVANCE A25, Bruker,

United States). The sample was scanned from 10° to 30° with a scan rate of 0.02°/s. The grain size D can be calculated by the Scherrer equation of $D = \kappa\lambda/\omega\cos\theta$, where κ is the Scherrer constant; herein, κ is set to 0.89 because the MgO and BT nanoparticles are spherical; λ is the wavelength of X-ray, 0.15406 nm; ω is the half peak width of diffraction peak; and θ is the Bragg angle.

The dielectric properties of the films were tested by using a broadband dielectric spectrometer (Concept 80, Novocontrol Technologies, Germany) with a frequency range from 10^{-1}–10^{7} Hz at room temperature. The diameters of the sputtering gold electrode of the upper and lower surfaces for each sample are 30 and 40 mm, respectively. A computer-controlled voltage breakdown test system (HJC-100kV, Huayang Instrument Co., Ltd., China) was used to test the breakdown strength of films. The test is carried out by placing the specimen between two spherical electrodes with a voltage step-up rate of 1 kV/s. The tests were repeated 20 times for each specimen at different positions. The ferroelectric test system (Radiant Precision Premier II, Radiant Technology, United States) was used to test the *D-E* loops of samples with a diameter of the sputtering gold electrode of 30 mm on both sides, under the electric field with an alternating frequency of 100 Hz and strength of 60 kV/mm. The electrical conductivity of films was measured using an electrometer (6517A Electrometer, Keithley, Cleveland, OH, United States) with a system of three-terminal electrodes. Under the applied electric field of 300 V, the tests were repeated 11 times for each specimen at room temperature.

2.3 Model

The two-dimensional structure models of PP-based nanocomposite dielectrics were established by the Monte Carlo method. The structural models consist of two phases of polymer matrix and nanoparticles. The nanoparticles were uniformly distributed in the polymer matrix.

If the applied electric field is relatively low, the space charge cannot be considered in the dielectrics, so the electric displacement can be given by

$$\nabla \cdot \mathbf{D}(\mathbf{r}) = 0, \tag{3}$$

where $\mathbf{D}(\mathbf{r})$ is the electric displacement at any position in the nanocomposites.

Substituting the constitutive equation $\mathbf{D}(\mathbf{r}) = \varepsilon(\mathbf{r})\mathbf{E}(\mathbf{r})$ into **Equation 3**, we can get the generalized Poisson equation after representing the electric field by the negative gradient of the electric potential

$$\nabla \cdot \mathbf{D}(\mathbf{r}) = \nabla \cdot (\varepsilon(\mathbf{r})\mathbf{E}(\mathbf{r})) = \nabla \cdot [\varepsilon(\mathbf{r})(-\varphi(\mathbf{r}))] = 0, \tag{4}$$

where $\varepsilon(\mathbf{r})$, $\mathbf{E}(\mathbf{r})$, and $\varphi(\mathbf{r})$ are the permittivity, electric field, and electric potential at any position in the nanocomposites, respectively.

The finite-volume scheduled relaxation Jacobian iterative method can quickly solve **Equation 4**. Then the electric field $\mathbf{E}(\mathbf{r})$ and electrostatic energy $U(\mathbf{r})$ can be calculated by $\mathbf{E}(\mathbf{r}) = -\varphi(\mathbf{r})$, $U(\mathbf{r}) = \frac{1}{2}\varepsilon_0\varepsilon_r(\mathbf{r})|\mathbf{E}(\mathbf{r})|^2$, respectively, where $\varepsilon_r(\mathbf{r})$ is the relative permittivity at any position in the nanocomposites.

3 EXPERIMENTAL RESULTS AND DISCUSSION

Figure 2A shows the cross-sectional SEM image of B with a BT content of 45 wt%; the plenty of nanoparticles are evenly distributed on the cross section. It can be seen from **Figure 2B**, **C** that the sandwich-structured films were successfully prepared, and the A, B layers were closely connected without cracks and obvious defects. The thickness ratio of the A, B, and A three layers in ABA-structured film is roughly 1:2:1, and the thickness of the middle layer is about 50 μm. The thickness ratio of B, A, and B three layers in BAB-structured film is roughly 1.5:1:1.5, and the thickness of the middle layer is about 25 μm. The particle size and particle spacing of BT nanoparticles in the PP matrix were statistically analyzed by ImageJ software. The average spacing values between nanoparticles of PP/BT nanocomposite dielectrics with BT contents of 10, 20, 30, 40, and 55 wt% are 797, 560, 383, 197, and 195 nm, respectively. It indicates the particle spacing decreases along with the increase in the BT content.

The frequency-dependent relative permittivity of ABA, BAB, B, A, and pure PP is shown in **Figure 3**. For the ABA-structured nanocomposite films, the relative permittivity increases gradually with the increase in the BT content in polarization layers (**Figure 3A**). The difference in relative permittivity of ABA-structured films is not obvious when the BT content is low. When the BT content reaches 30 wt%, the relative permittivity increases significantly. The increase in relative permittivity is nonlinear with the increment of the BT content (Fan et al., 2012; Zhong et al., 2018). This is because when the BT content is higher than 30 wt%, the increasing density of BT nanoparticles significantly reduces the nanoparticle spacing. Meanwhile, the relative permittivity in the low-frequency region is found to be higher than that in the high-frequency region, and this difference increases with the increment of the BT content. The reason is that the interlayer polarization is enhanced when the BT content is high; correspondingly, the relative permittivity in the low-frequency region increases.

The variations of relative permittivity with BT contents and frequency of BAB-structured and B films are similar to those of ABA (**Figure 3A–C**). At the same BT content, the order of the relative permittivity from large to small is B > BAB > ABA > pure PP > A. The single-layered A is the PP/MgO nanocomposites with the MgO content of 0.5 wt%. When a small amount of MgO nanoparticles are doped into the PP matrix, the independent interfacial regions will be formed in the PP-based nanocomposite dielectrics. The molecular chain motions will be hindered, and dipolar turning will be inhibited in the interfacial regions. Therefore, the relative permittivity of A is the smallest. The sandwich-structured PP-based nanocomposite dielectric can be regarded as a "parallel capacitor". The B layer contains BT nanoparticles with high permittivity, so its capacitance is much larger than that of the A layer. For the ABA-structured

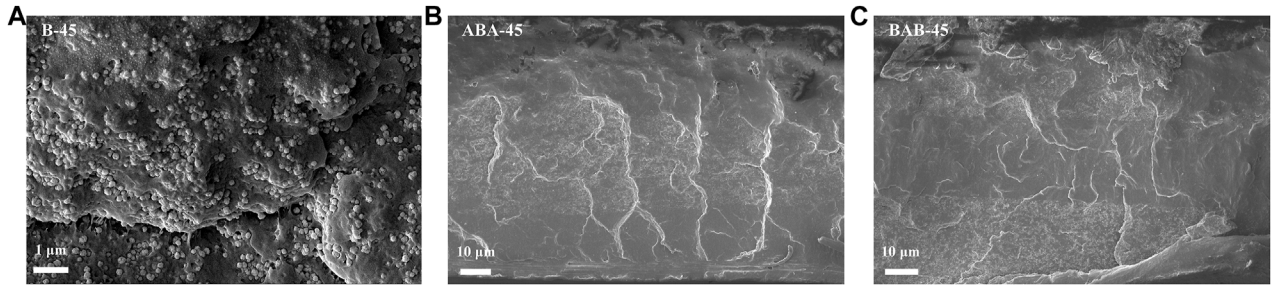

FIGURE 2 | Cross-sectional SEM images of B-45 **(A)**, ABA-45 **(B)**, and BAB-45 **(C)**.

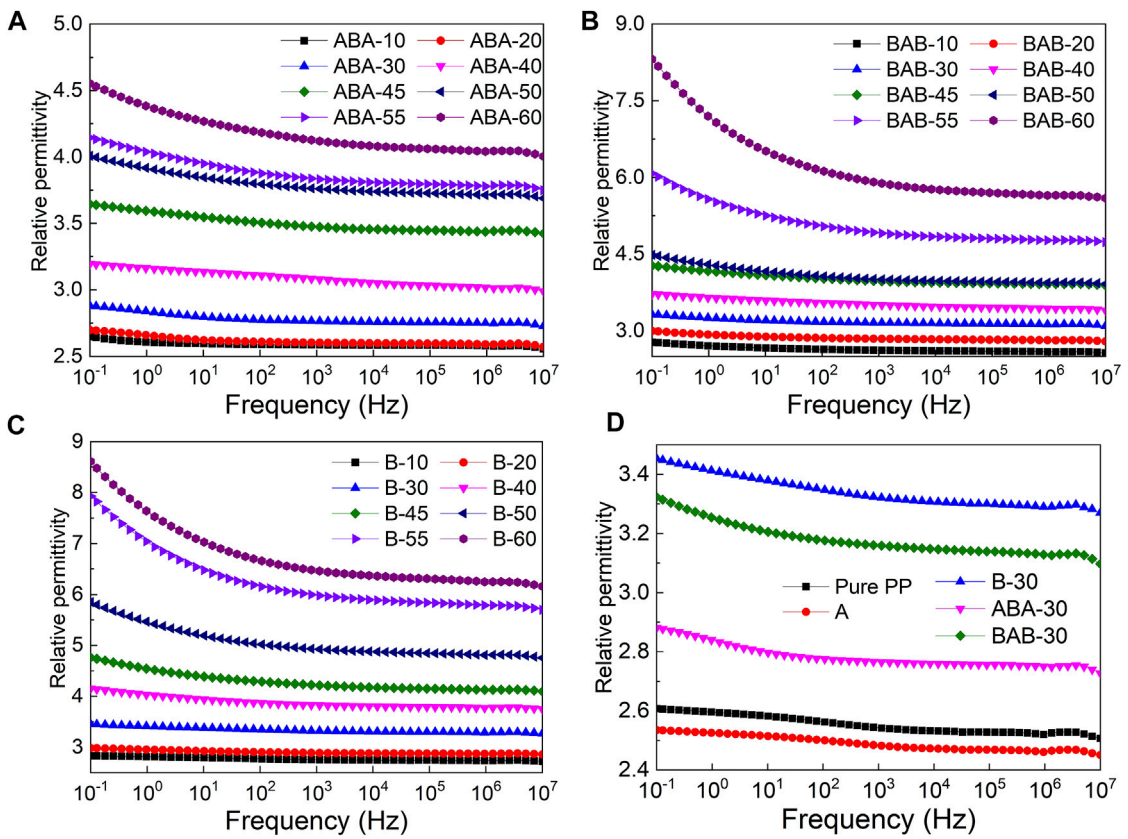

FIGURE 3 | Dependence of relative permittivity on frequency for **(A)** ABA, **(B)** BAB, **(C)** B, and **(D)** pure PP, A, B-30, ABA-30, and BAB-30.

nanocomposite dielectric, it is equivalent to two capacitors A and one capacitor B in parallel. Although, the BAB-structured nanocomposite dielectric is equivalent to two capacitors B and one capacitor A in parallel. Therefore, the capacitance of the BAB-structured nanocomposite dielectric is larger than that of the ABA-structured nanocomposite dielectric.

The dependences of dielectric loss on frequency for ABA, BAB, B, A, and pure PP are shown in **Figure 4**. It can be seen from **Figure 4A** that the dielectric loss of the ABA-structured films gradually increases with the increase in the BT content. However, the maximum dielectric loss is still lower than 0.04, which indicates that the ABA-structured films have good dielectric stability. The dielectric loss in the low-frequency region is mainly caused by the organic-inorganic interface polarization, orientation polarization of the dipole, and interlayer polarization. In **Figure 4A**, the relaxation peak shifts to the right with the BT content increasing from 10 to 40 wt%. The relaxation peak corresponds to the interlayer polarization. The establishment time of the interlayer polarization can be given by $\tau = \varepsilon_0\varepsilon_r/\sigma$, where the σ is the electrical conductivity. As the BT content increases from 10 to 40 wt%, the growth rate of conductivity is greater than that of the permittivity; therefore, the establishment

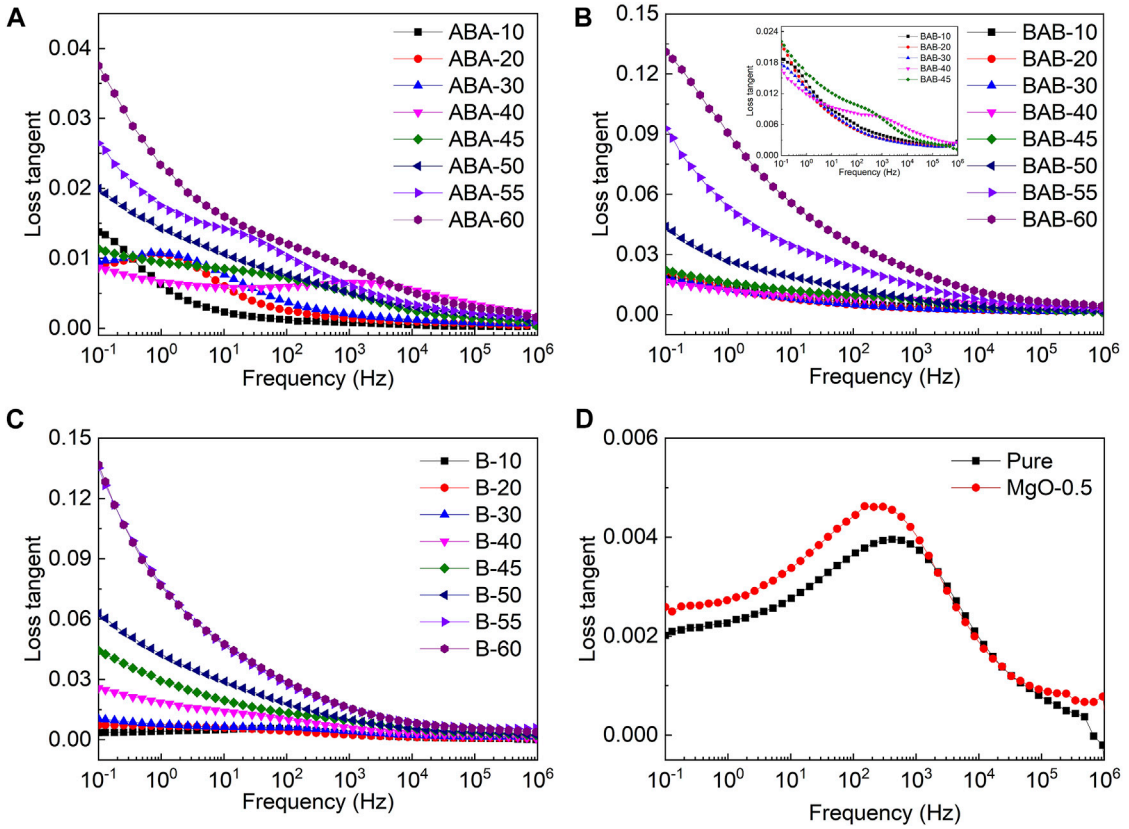

FIGURE 4 | Dependence of dielectric loss on frequency for ABA **(A)**, BAB **(B)**, B **(C)**, and **(D)** pure PP and **(A).**

time of the interlayer polarization decreases. As a result, the relaxation peak shifts to the right. In **Figure 4A,B**, as the BT content in the B layer increases, the increment of loss tangent for films with BT contents larger than 45% is significantly higher than that for films with lower contents. A large content of BT nanoparticles increases the permittivity and capacitance of the B layer, which causes a more intensive ε_r difference between adjacent layers and an enhanced interlayer polarization. On the whole, especially at high BT contents, the dielectric loss tangent of the ABA films is smaller than that of BAB films which is smaller than that of B. It corresponds to the ordering of the relative permittivity, where a large polarization strength corresponds to a large dielectric loss.

Figure 5 shows the Weibull distribution of DC breakdown strength and shape parameter of ABA, BAB, B, A, and pure PP. As shown in **Figure 5A**, the Weibull breakdown distribution of the ABA-structured films is more concentrated when the BT content is between 10 and 45 wt%, indicating that the breakdown strength of the films does not change much in this content range. The breakdown strength of ABA begins to decrease sharply when the BT content reaches 45 wt% (**Figure 5E**). The breakdown strength of the BAB-structured films decreases linearly with the increase in the BT nanoparticle concentration. As the BT content increases from 10 wt% to 60 wt%, the breakdown strength of BAB-structured films decreases from 466.99 kV/mm to 303.25 kV/mm (**Figure 5E**). It can be seen from **Figure 5C** that the Weibull breakdown distribution of the single-layered B films is concentrated at 10, 20, and 30 wt% of the BT content. When the breakdown strength decreases significantly, the BT content is higher than 30 wt%. At the BT content of 10 wt%, ABA, BAB, and B have the largest breakdown strength of 466.54, 466.99, and 385.63 kV/mm, respectively. The breakdown strength of these decreases significantly at a high BT content, which is because the breakdown strength of the BT nanoparticles is relatively low. The large content of BT can weaken the breakdown performance of the PP-based nanocomposites. On the whole, the shape parameters of the sandwich-structured films are smaller than that of the single-layer films (**Figure 5F**), which indicates that the uniformity of sandwich-structured films decreases slightly. **Figure 5E** shows that A has the largest breakdown strength of 490 kV/mm, which is 20.8% higher than that of pure PP. In total, the order of the breakdown strength of samples is A > ABA > BAB > B. It illustrated that the sandwich structures of ABA and BAB can alleviate the damage of BT nanoparticles on the breakdown performance of nanocomposite dielectrics, which is benefited from the A layer in the sandwich structures. The A layer with the highest breakdown strength can mitigate the low breakdown effect caused by the B layer. It demonstrates that sandwich structures can synergistically increase the relative permittivity and breakdown strength.

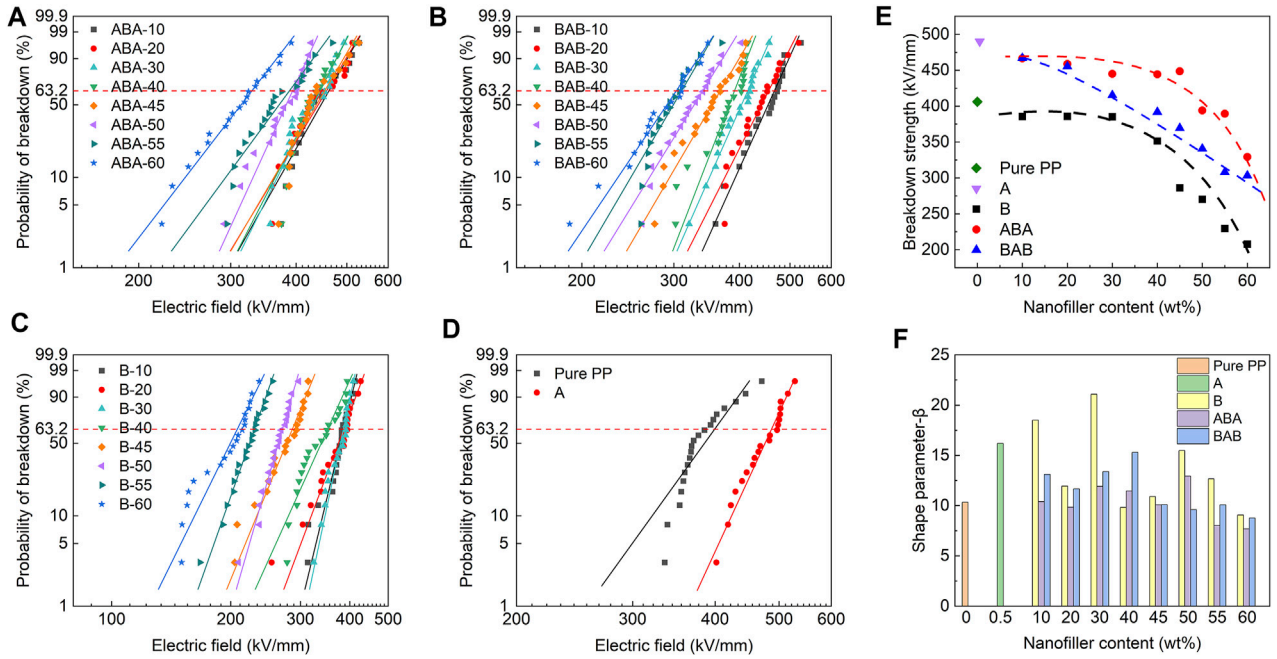

FIGURE 5 | Weibull distribution of the DC breakdown strength of ABA **(A)**, BAB **(B)**, B **(C),** and **(D)** A and pure PP. The Weibull breakdown strength **(E)** and shape parameter **(F)** of pure PP, single-layered A, B, sandwich-structured ABA, and BAB films.

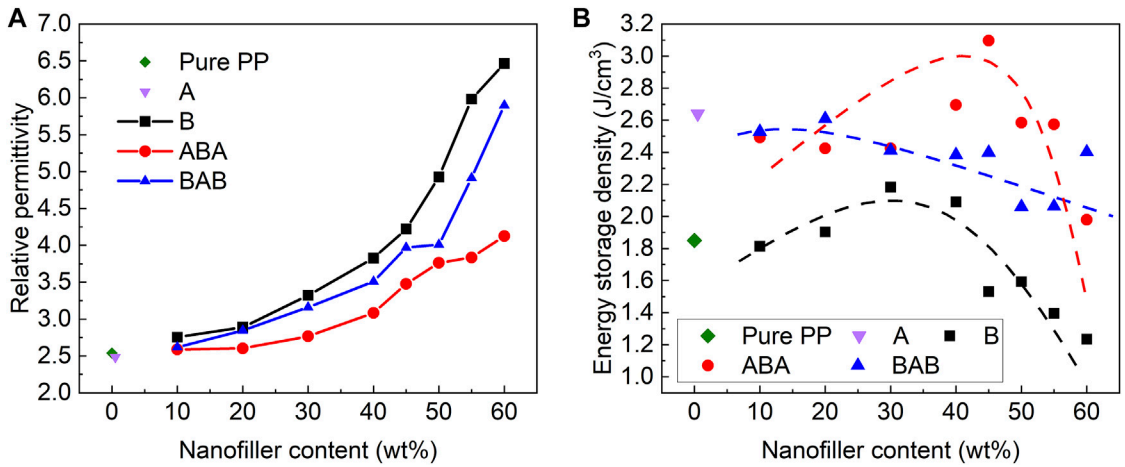

FIGURE 6 | Relative permittivity at 1 kHz **(A)** and energy density **(B)** of Pure PP, single-layered A, B, sandwich-structured ABA, and BAB films. The energy density was calculated by the relative permittivity at 1 kHz and Weibull breakdown strength.

Based on the energy density formula of linear dielectrics, the energy density of pure PP and PP-based nanocomposites can be calculated by using the breakdown strength (**Figure 5E**) and relative permittivity at 1 kHz (**Figure 6A**), as shown in **Figure 6B**.

The energy densities of ABA-structured films and B films exhibit a downward parabola trend with the increase of the BT content, reaching the maximum values of 3.10 and 2.18 J/cm^3 at the BT contents of 45 wt% and 30 wt%, respectively. The energy density of BAB-structured films decreases roughly linearly as the BT content increases, with the maximum value of 2.61 J/cm^3. However, the energy density of pure PP is only 1.85 J/cm^3. Both the sandwich structures of ABA and BAB can improve the energy density of PP. The ABA structure is more effective in improving the energy density, which is about 67% higher than that of pure PP. The BAB structure increases the energy storage density of PP by 41%.

To further compare the energy storage performance of PP-based nanocomposite dielectrics with different structures, *D-E*

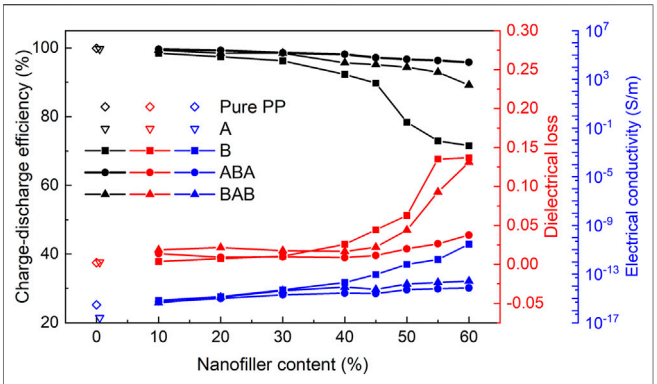

FIGURE 7 | Charge-discharge efficiency, dielectric loss at 0.1 kHz, and electrical conductivity for pure PP, single-layered A, B, sandwich-structured ABA, and BAB films. The charge-discharge efficiency of the samples was obtained by the D-E loop tests which were conducted under the electric field with an alternating frequency of 100 Hz and strength of 60 kV/mm.

loops were measured under the electric field with an alternating frequency of 100 Hz and strength of 60 kV/mm to obtain the charge-discharge efficiencies of samples. The charge-discharge efficiency, dielectric loss tangent at 0.1 kHz, and electrical conductivity for pure PP, single-layered A, B, sandwich-structured ABA, and BAB films are shown in **Figure 7**.

In **Figure 7**, it can be clearly seen that as the BT content increases, the charge-discharge efficiencies of B, ABA, and BAB films decrease, and the dielectric loss at 0.1 Hz and the electrical conductivity of those films increase gradually. As the BT content increases from 10 to 60 wt%, the charge-discharge efficiency decreases from 98.4% to 71.6% for B films, from 99.6 to 95.8% for ABA films and from 99% to 89.1% for BAB films. The ABA films exhibit optimal energy storage efficiency. Under the same content of BT nanoparticles in the B layer, the order of the dielectric loss at 0.1 Hz and electrical conductivity are roughly B > BAB > ABA, and the order of charge-discharge efficiency is ABA > BAB > B. In particular, between the charge-discharge efficiency and the electrical conductivity, there is a good correspondence. The electrical conductivity is the key factor affecting the charge-discharge efficiency. High electrical conductivity will result in a large leakage current in the material, which can generate a large amount of Joule heat, leading to significant energy loss. The dielectric loss can also cause energy loss. It means the released energy will decrease, eventually leading to a decrease in the charge-discharge efficiency.

The sandwich-structured nanocomposite can be regarded as a "series circuit". The ABA-structured dielectric is equivalent to two A impedances with a B impedance in series. The BAB-structured dielectric is equivalent to two B impedances with an A impedance in series. The electrical conductivity of A is 2.57×10^{-17} S/m, which is lower than that of B, so the electrical conductivity of ABA and BAB is larger than that of B but smaller than that of A. Also, because there are two layers of A in ABA and only one layer of A in BAB, the electrical conductivity of ABA is smaller than that of BAB. Lower electrical conductivity means lower energy loss and higher charge-discharge efficiency.

In summary, the sandwich structures can reduce the electrical conductivity and dielectric loss of PP-based nanocomposites, leading to the improvement of the charging-discharging efficiency. Under the same BT content in B layer, the ABA films have lower conductivity and higher charge-discharge efficiency than those of BAB films. The single-layered B dielectric has the lowest charge-discharge efficiency.

4 BREAKDOWN MECHANISM AND SIMULATION

4.1 Breakdown Mechanism of Single-Layered Films

Since the square of the breakdown strength is proportional to the energy storage density, the breakdown strength has a greater effect on the energy storage density than the dielectric constant. Clarifying the breakdown mechanism of the PP-based nanocomposites with different structures can provide theoretical support for the design of dielectrics with high-energy storage performance. The breakdown mechanisms of single-layered films and sandwich-structured films are different; therefore, the breakdown mechanism of single-layered dielectric films is first analyzed.

Some studies have pointed out that the crystalline performance has an important impact on the breakdown properties of PP-based nanocomposite dielectrics because the crystalline can reflect the microstructure of the PP dielectrics, and the change in the microstructures can affect the movement of the molecular chains, which can adjust the breakdown path (Mi et al., 2020). Therefore, the crystalline and breakdown performances of single-layered films are investigated here.

In **Figure 8**, it can be seen that the breakdown strength of single-layered A films is 490 kV/mm, which is much higher than that of single-layered B films. The mass crystallinity of A film is about 47.97%, and the grain size is 29.53 nm. With the increase of the BT content, the breakdown strength and the crystallinity of B films first remain approximately constant and then decrease, while the grain size shows an increasing trend. At the BT contents of 10, 20, and 30 wt% for B films, the breakdown strength lies between 385.23 and 385.81 kV/mm, which are nearly constant. As the BT content of the B films increase from 40 to 60 wt%, the breakdown strength decreases from 351.37 to 207.70 kV/mm sharply. The crystallinities are between 44.06% and 51.10% as a whole and begin to decrease slightly at the BT concentration of 45%. The range of grain sizes is between 29.43 and 39.41 nm, showing an overall positive correlation with the BT content. The decrease in crystallinity and the increase in the grain size imply a decrease in crystalline boundaries. There are many deep traps in the amorphous-crystalline interfaces, which can hinder the transport of carriers and reduce the electron mean free path, leading to an increase in the breakdown strength (Wang et al., 2016). However, as the BT content increases, the amorphous-crystalline interfaces decrease, which reduces the breakdown strength. In addition, the large difference in dielectric constants between PP and BT causes electric field distortion. This distortion is aggravated by the larger

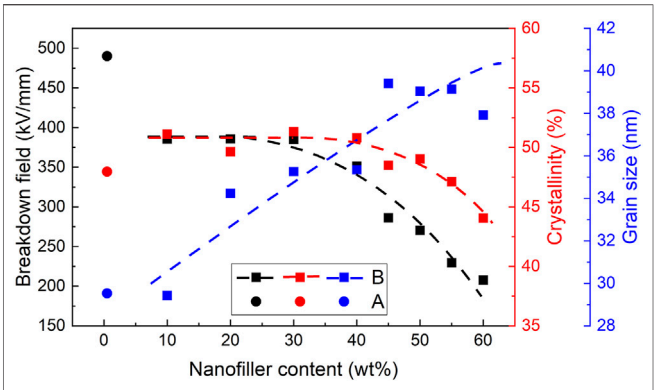

FIGURE 8 | Breakdown strength, crystallinity, and the size of a grain of single-layered A and B films. The crystallinity was obtained by DSC tests, and the grain size was obtained by XRD tests.

BT content, and the uneven electric field distribution leads to the breakdown of the nanocomposites.

The breakdown strength of A films is 490 kV/mm, which is much higher than that of B films and 20.8% higher than that of pure PP (**Figure 5E**, **Figure 8**). The electrical conductivity of A film is the lowest among all the samples (**Figure 7**). There are three reasons for the excellent insulating properties of A films. First, the difference in relative permittivity of pure PP and MgO nanoparticles is not significant, so the electric field distortion between PP and MgO is not serious. Second, mixing a small amount of nanoparticles into PP can introduce the interfacial regions with deep traps, which can enhance the ability of traps to capture carriers and decreases the electrical conductivity. The reduction of charge injection and carrier transport will reduce the space charge accumulation and moderate the electric field distortion inside the nanocomposite dielectric. Third, the binding effect of nanoparticles on molecular chains in the interfacial region can hinder the expansion of free volume, which reduces the electron mean free path and the breakdown strength.

4.2 Breakdown Mechanism of Sandwich-Structured Films

The breakdown mechanism of PP-based nanocomposites with sandwich structures is different from that of single-layered structures. The breakdown mechanism of nanocomposite dielectrics with sandwich structures cannot be explained simply by the breakdown mechanism of single-layered dielectrics. Considering the electric field distribution and charge transport, the breakdown characteristics of ABA- and BAB-structured PP-based nanocomposites are analyzed. **Figure 9** gives a schematic diagram of the electric field distribution of the single-layered and the sandwich-structured PP-based nanocomposites.

In **Figure 9**, when the same electric field is applied to PP-based nanocomposites with different structures, the electric field distributions inside those dielectrics are different. The electric field distributions of single-layered A and B films are the same. The intensity of the electric field inside the sample does not vary with the position. However, the electric field distributions inside ABA and BAB structured films are different. For the two sandwich-structured films, the electric field intensity of the A layer is higher than that of the B layer. There is a lower electric field in the B layer than that in the single-layered B film. 1) The A layer in ABA can increase the charge injection barrier at the interfaces between the electrode and A layer, which reduces the charge injection. 2) The interfaces between the A layer and B layer can hinder the charge transport from the B layer to the A layer, thus causing the charge mobility of sandwich-structured

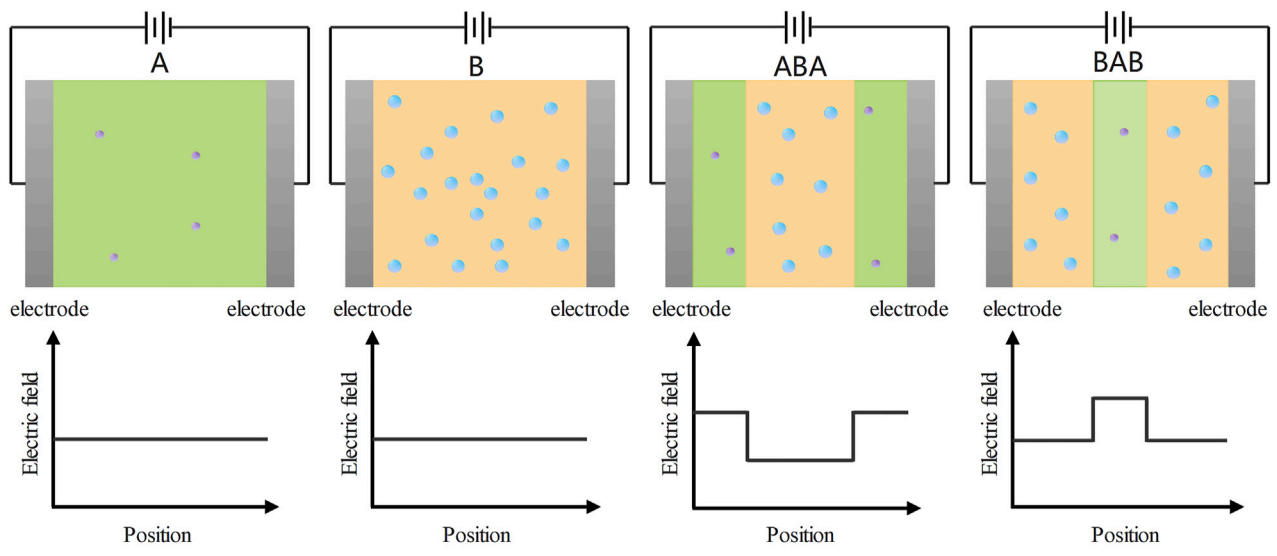

FIGURE 9 | Under the action of the applied electric field, the electric field distributions inside the PP-based nanocomposites with sandwich structures and single-layered structures.

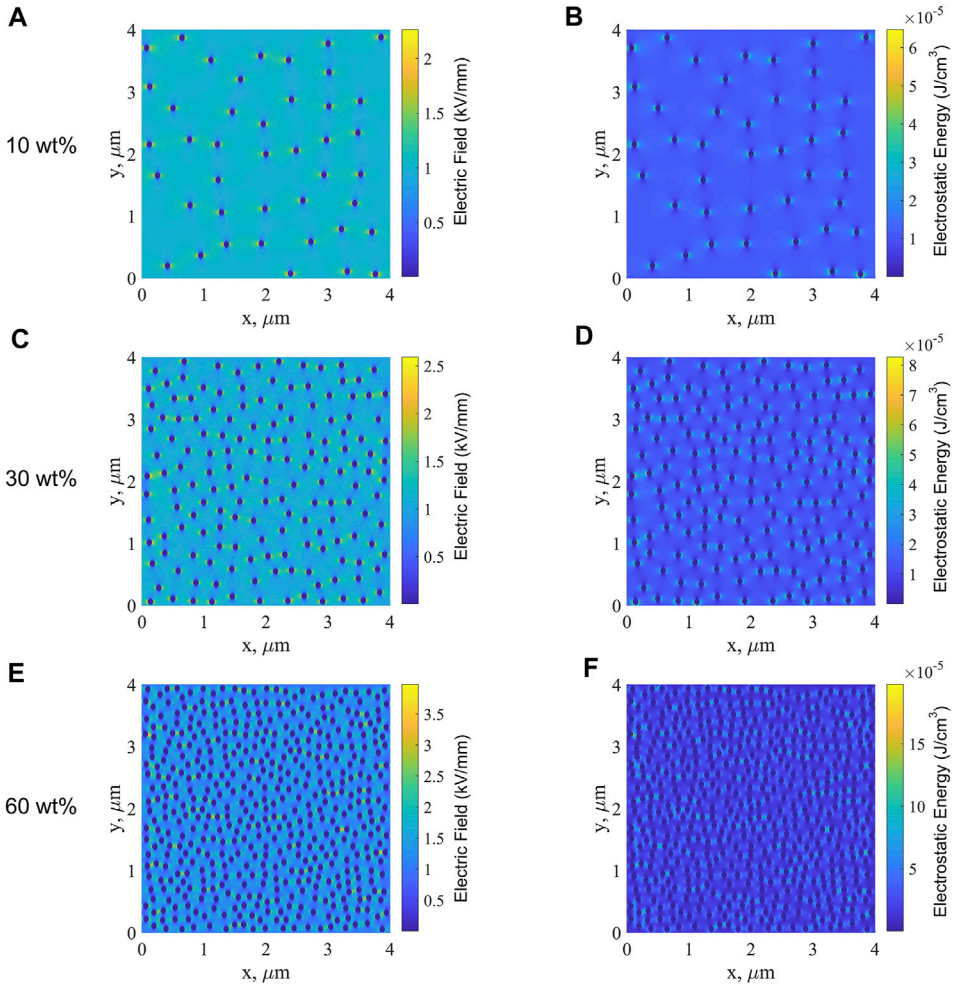

FIGURE 10 | Electric field along the *x*-direction of single-layered B films with BT contents of 10 wt% **(A)**, 30 wt% **(C)**, and 60 wt% **(E)** and the electrostatic energy of single-layered B films with BT contents of 10 wt% **(B)**, 30 wt% **(D)**, and 60 wt% **(F)**.

dielectrics to become lower than that of single-layered B dielectrics. 3) The decreases in charge injection and charge mobility reduce the space charge accumulation in sandwich-structured dielectrics, resulting in larger breakdown strength of sandwich-structured films than that of single-layered B film. Consequently, the ABA and BAB-structured PP-based nanocomposite dielectrics exhibit superior breakdown properties to single-layered B dielectrics.

Combined with the experimental results of breakdown strength mentioned in **Figure 5**, it can be seen that the breakdown strength of ABA is higher than that of BAB at the same BT content in the B layer. The outer layer of ABA-structured dielectrics is the A layer that the PP/MgO nanocomposite dielectric with the MgO content of 0.5 wt%. A layer can increase the barrier of charge injection at the interface between the ABA sample and the electrode, causing a decrease in the number of charges injected from the electrode to the sample and then leading to the reduction of charges migrated to the B layer. The interface between A and B layers also causes the charge mobility in the middle B layer of ABA films to be slower than that in B film at the same BT content. For BAB structured films, the middle A layer can increase the barrier at the interface between the A and B layers, which hinders the charge migration inside the BAB samples and then improves the breakdown strength. The ABA structure can reduce the charges injected into the PP-based nanocomposites at the source. The BAB structure cannot reduce the charges injected into the PP-based nanocomposites effectively. The middle A layer of BAB films acts as a "buffer" to reduce the charge mobility inside the BAB film. In consequence, the ABA structure can improve the breakdown strength of PP-based nanocomposites to a greater extent, which is more advantageous for energy storage.

4.3 Simulation of the Electric Field and Electrostatic Energy

The simulation of the fluctuation of electric field and electrostatic energy can be used to analyze the breakdown characteristics of

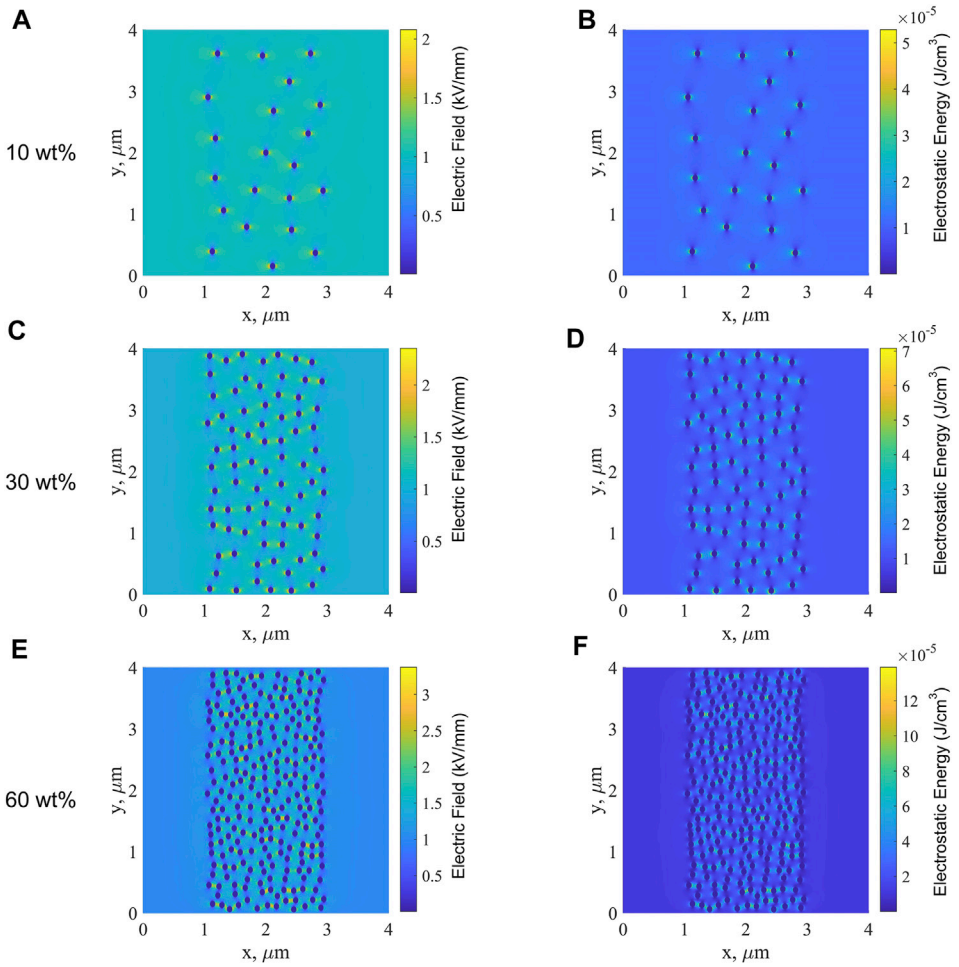

FIGURE 11 | Electric field along the *x*-direction of sandwich-structured ABA films with BT contents of 10 wt% **(A)**, 30 wt% **(C)**, 60 wt%, and **(E)** in the B layer and the electrostatic energy of ABA films with BT contents of 10 wt% **(B)**, 30 wt% **(D)**, and 60 wt% **(F)** in the B layer.

single-layered and sandwich-structured PP-based nanocomposites. The simulations were simulated for single-layered and sandwich-structured films with different BT contents in the B layer, and the effects of different BT contents on the breakdown performance of PP-based nanocomposite dielectrics were obtained. The simulation parameters were set as follows: the density of PP is 0.9 g/cm^3, and the density of BT nanoparticles is 5.85 g/cm^3. The relative permittivities of PP and BT nanoparticles are 2.54, and 900, respectively. The A layer is the PP/MgO nanocomposite with a MgO content of 0.5 wt%, whose filler content is small. Hence, the A layer can be regarded as a homogenous material, and its relative permittivity is 2.48. The radius of BT particles is set as 45 nm. From the SEM image of PP-based nanocomposites (**Figure 2**), it is known that the BT nanoparticles have good dispersibility in the PP matrix. Therefore, the parameter characterizing the dispersion of nanoparticles was set to 10. The larger value of the parameter indicates the better dispersion of nanoparticles in the matrix, while the smaller value of the parameter indicates the more severe agglomeration of nanoparticles in the matrix. The thickness of single-layered and sandwich-structured films was set to 4 μm. The applied voltage was set to 4 V, and the macroscopic electric field strength is 1 kV/mm.

By changing the concentration of BT nanoparticles, the two-dimensional electric field and electrostatic energy distributions were obtained for single-layered and sandwich-structured PP-based nanocomposites, as shown in **Figures 10–12**. Based on the simulated results, the breakdown mechanism of PP-based nanocomposite dielectrics can be further analyzed.

First, the simulation results of single-layered B films are analyzed. **Figure 10A, C, E** show the distribution of the electric field along the *x*-direction inside the single-layered B film at BT contents of 10, 30, and 60 wt%, respectively. Because the relative permittivity of BT nanoparticles is much higher than that of PP; in consequence, the electric field along the *x*-direction of BT nanoparticles is much lower than that of the PP matrix. The electric field between the PP matrix and the BT nanoparticles is higher than that of the PP matrix, which is caused by the polarization induced by the doped BT nanoparticles. As the BT content increases, the electric field between BT

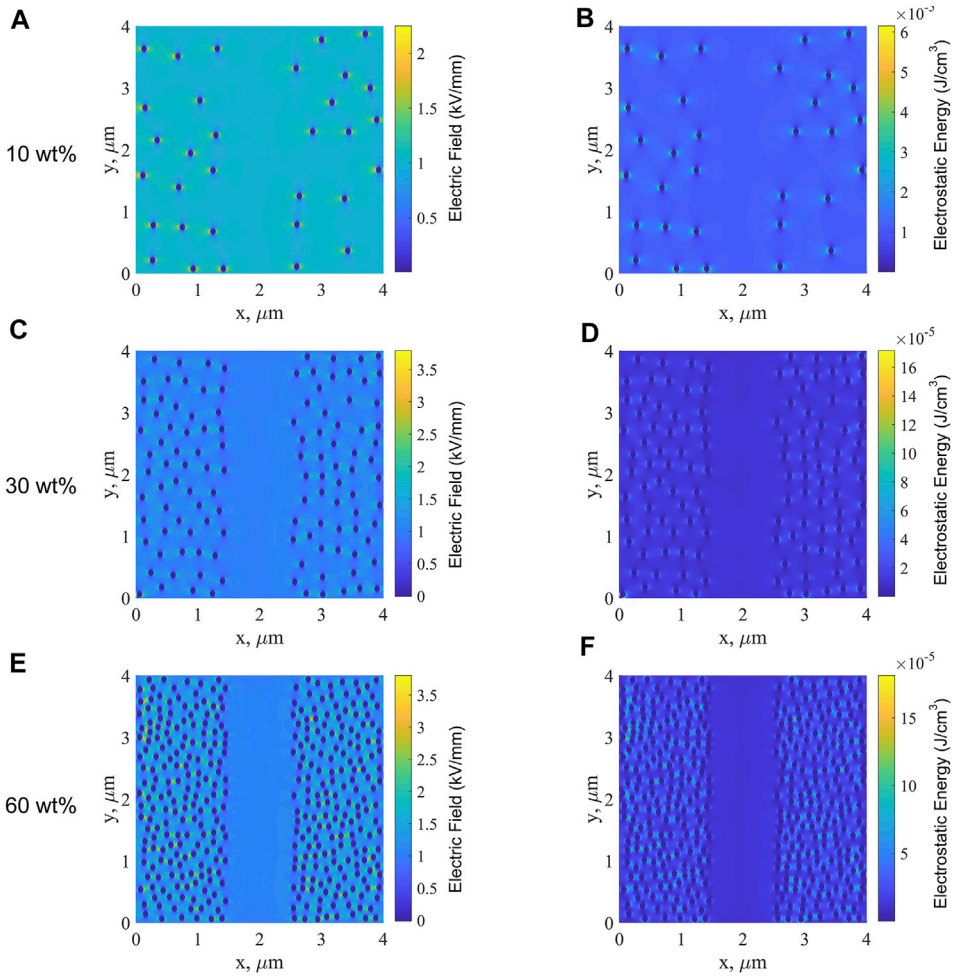

FIGURE 12 | Electric field along the *x*-direction of sandwich-structured BAB films with BT contents of 10 wt% **(A)**, 30 wt% **(C)**, and 60 wt% **(E)** in the B layer and the electrostatic energy of BAB films with BT contents of 10 wt% **(B)**, 30 wt% **(D)**, and 60 wt% **(F)** in the B layer.

nanoparticles and the PP matrix becomes larger, indicating the enhancement of polarization between nanoparticles and matrix. At the higher content of nanoparticles, the polarization region begins to overlap, and conductive channels are formed more easily. **Figure 10B,D,F** show the electrostatic energy of single-layered B films. The electrostatic energy between the BT nanoparticles and PP matrix is larger than that of the PP matrix larger than that of BT nanoparticles. Similar to the electric field along the *x*-direction, the electrostatic energy between nanoparticles and matrix becomes larger with the increase of the BT content, namely, the electrostatic energy of the polarization region is higher. The higher the polarization intensity is, the greater is the electrostatic energy, and accordingly, the greater the energy loss will be. In consequence, under the action of a strong electric field, the current density in the B films will increase sharply with the increase in the BT content, which leads to the surge of local Joule heat, resulting in the decrease of breakdown field strength.

Figure 11 shows the electric field along the *x*-direction and electrostatic energy of the sandwich-structured ABA films with BT contents of 10, 30, and 60 wt% in the B layer. In **Figure 11**, in the middle B layers, the electric field between the nanoparticle and matrix is high and the polarization is strong, which is consistent with that observed from the simulated results for single-layered B films. The content of MgO nanoparticles in the A layer is only 0.5 wt%, which is very small. The layer A can be regarded as a homogenous material with a low dielectric constant, as explained in the part of the simulation parameter setting. Therefore, it can be seen that the electric field at layer A is low. With the increase in the BT content, only the electric field between nanoparticles and the PP matrix at the middle layer B increases, the electric field of layer A on both sides is still very low, as is the electrostatic energy of layers A and B. Consequently, it is more difficult to establish a conductive path in the PP-based nanocomposite dielectric with the ABA structure than that in the single-layered B film. As the BT content increases, the electric field along the *x*-direction and the electrostatic energy in the middle layer B increases significantly, making the dielectric more prone to breakdown. Hence the breakdown strength of ABA films decreases with the increase in the BT content.

Figure 12 shows the electric field along the *x*-direction and the electrostatic energy of the sandwich-structured BAB films with BT contents of 10, 30, and 60 wt% in the B layer. It can be seen from **Figure 12** that the electric field and electrostatic energy of the middle layer A are low and those of layers B on both sides are high. As the BT content increases, the distance between the nanoparticles becomes smaller; the electric field distortion becomes more serious and the corresponding electrostatic energy surges. The breakdown strength of BAB decreases with the increase in the BT content.

At the same BT content in the B layer, the region with a high electric field along the *x*-direction and high electrostatic energy in BAB films is larger than that in the ABA layer. As a result, the conductive path in BAB films is easier to be established than that in ABA films, and the energy loss is more serious in BAB films. Consequently, at the same BT content, the breakdown strength of BAB is lower than that of ABA films. In conclusion, under the same BT content in the B layer, the breakdown strength of PP-based nanocomposite dielectrics with the ABA structure is larger than that with the BAB structure than that with the B structure.

5 CONCLUSION

The PP/MgO nanocomposite dielectric with the MgO content of 0.5 wt% was employed as the high breakdown film, which was referred to as "A". The PP/BT nanocomposite dielectrics with various BT contents were employed as high polarization films, which were referred to as "B". The single-layered, ABA-structured, and BAB-structured PP-based nanocomposite dielectrics were prepared by melting, blending, and hot-pressing methods. The order of relative permittivity is roughly B > BAB > ABA > pure PP > A when the BT content is the same in the B layer. For sandwich-structured dielectrics, the polarization layer and interface between the adjacent layers can increase the polarization strength of dielectrics. At the lower BT content, the order of breakdown strength is A > ABA > BAB > pure PP > B. The high breakdown layer and barrier at the interface between the adjacent layers can reduce the charge mobility and the charge injection. In addition, the sandwich structures can redistribute the electric field, resulting in a lower electric field in the B layer than that in the single-layered B film. Therefore, the sandwich structures can synergistically improve the dielectric constant and breakdown strength of PP-based nanocomposite dielectrics, leading to an increase in the energy density. The energy density of ABA-structured PP nanocomposite dielectrics with the BT content of 45wt% in B layer is 3.09 J/cm^{-3}, which is 67% higher than that of pure PP. The work provides a new concept for improving the energy storage performance of polymer nanocomposite dielectrics *via* macroscopic and mesoscopic structure designs.

DATA AVAILABILITY STATEMENT

The original contributions presented in the study are included in the article/Supplementary Material, further inquiries can be directed to the corresponding authors.

AUTHOR CONTRIBUTIONS

All authors listed have made a substantial, direct, and intellectual contribution to the work and approved it for publication.

FUNDING

This work was supported by the National Natural Science Foundation of China (Grant Nos. 52077162 and U1830131).

REFERENCES

Ai, D., Li, H., Zhou, Y., Ren, L., Han, Z., Yao, B., et al. (2020). Tuning Nanofillers in *In Situ* Prepared Polyimide Nanocomposites for High-Temperature Capacitive Energy Storage. *Adv. Energy Mat.* 10 (16), 1903881. doi:10.1002/aenm.201903881

Chen, Q., Shen, Y., Zhang, S., and Zhang, Q. M. (2015). Polymer-based Dielectrics with High Energy Storage Density. *Annu. Rev. Mat. Res.* 45 (1), 433–458. doi:10.1146/annurev-matsci-070214-021017

Dang, Z.-M., Lin, Y.-Q., Xu, H.-P., Shi, C.-Y., Li, S.-T., and Bai, J. (2008). Fabrication and Dielectric Characterization of Advanced BaTiO3/Polyimide Nanocomposite Films with High Thermal Stability. *Adv. Funct. Mat.* 18 (10), 1509–1517. doi:10.1002/adfm.200701077

Dang, Z.-M., Yuan, J.-K., Yao, S.-H., and Liao, R.-J. (2013). Flexible Nanodielectric Materials with High Permittivity for Power Energy Storage. *Adv. Mat.* 25 (44), 6334–6365. doi:10.1002/adma.201301752

Fan, B.-H., Zha, J.-W., Wang, D.-R., Zhao, J., and Dang, Z.-M. (2012). Experimental Study and Theoretical Prediction of Dielectric Permittivity in BaTiO3/polyimide Nanocomposite Films. *Appl. Phys. Lett.* 100 (9), 092903. doi:10.1063/1.3691198

Fang, X., Liu, X., Cui, Z.-K., Qian, J., Pan, J., Li, X., et al. (2015). Preparation and Properties of Thermostable Well-Functionalized Graphene Oxide/polyimide Composite Films with High Dielectric Constant, Low Dielectric Loss and High Strength via *In Situ* Polymerization. *J. Mat. Chem. A* 3 (18), 10005–10012. doi:10.1039/c5ta00943j

Ho, J., Ramprasad, R., and Boggs, S. (2007). Effect of Alteration of Antioxidant by UV Treatment on the Dielectric Strength of BOPP Capacitor Film. *IEEE Trans. Dielect. Electr. Insul.* 14 (5), 1295–1301. doi:10.1109/TDEI.2007.4339492

Jiang, J., Shen, Z., Cai, X., Qian, J., Dan, Z., Lin, Y., et al. (2019). Polymer Nanocomposites with Interpenetrating Gradient Structure Exhibiting Ultrahigh Discharge Efficiency and Energy Density. *Adv. Energy Mat.* 9 (15), 1803411. doi:10.1002/aenm.201803411

Li, H., Xie, Z., LiuLi, L., Peng, Z., Ding, Q., Ren, L., et al. (2019). High-performance Insulation Materials from Poly(ether Imide)/boron Nitride Nanosheets with Enhanced DC Breakdown Strength and Thermal Stability. *IEEE Trans. Dielect. Electr. Insul.* 26 (3), 722–729. doi:10.1109/TDEI.2018.00763710.1109/tdei.2019.8726017

Li, H., Yao, B., Zhou, Y., Xu, W., Ren, L., Ai, D., et al. (2020). Bilayer-structured Polymer Nanocomposites Exhibiting High Breakdown Strength and Energy Density via Interfacial Barrier Design. *ACS Appl. Energy Mat.* 3 (8), 8055–8063. doi:10.1021/acsaem.0c01508

Li, Q., Yao, F.-Z., Liu, Y., Zhang, G., Wang, H., and Wang, Q. (2018). High-temperature Dielectric Materials for Electrical Energy Storage. *Annu. Rev. Mat. Res.* 48 (1), 219–243. doi:10.1146/annurev-matsci-070317-124435

Liu, D., Wu, L., Wu, K., Xu, S., Sui, G., Jing, M., et al. (2019). Largely Enhanced Energy Density of Polypropylene Based Nanocomposites via Synergistic Hybrid

Fillers and High Shear Extrusion Assisted Dispersion. *Compos. Part A Appl. Sci. Manuf.* 119, 134–144. doi:10.1016/j.compositesa.2019.01.022

Liu, F., Li, Q., Cui, J., Li, Z., Yang, G., Liu, Y., et al. (2017). High-energy-density Dielectric Polymer Nanocomposites with Trilayered Architecture. *Adv. Funct. Mat.* 27 (20), 1606292. doi:10.1002/adfm.201606292

Liu, S., and Zhai, J. (2015). Improving the Dielectric Constant and Energy Density of Poly(vinylidene Fluoride) Composites Induced by Surface-Modified $SrTiO_3$ Nanofibers by Polyvinylpyrrolidone. *J. Mat. Chem. A* 3 (4), 1511–1517. doi:10.1039/c4ta04455j

Luo, H., Zhou, X., Ellingford, C., Zhang, Y., Chen, S., Zhou, K., et al. (2019). Interface Design for High Energy Density Polymer Nanocomposites. *Chem. Soc. Rev.* 48 (16), 4424–4465. doi:10.1039/c9cs00043g

Marwat, M. A., Xie, B., Zhu, Y., Fan, P., Ma, W., Liu, H., et al. (2019). Largely Enhanced Discharge Energy Density in Linear Polymer Nanocomposites by Designing a Sandwich Structure. *Compos. Part A Appl. Sci. Manuf.* 121, 115–122. doi:10.1016/j.compositesa.2019.03.016

Mi, R., Xing, Z., Hao, J., Hu, X., Min, D., Li, S., et al. (2020). Effect of Morphology and Traps on DC Conductivity and Breakdown of Polyethylene Nanocomposites. *IEEE Trans. Dielect. Electr. Insul.* 27 (2), 489–497. doi:10.1109/TDEI.2020.008583

Niu, Y., Xiang, F., Wang, Y., Chen, J., and Wang, H. (2018). Effect of the Coverage Level of Carboxylic Acids as a Modifier for Barium Titanate Nanoparticles on the Performance of Poly(vinylidene Fluoride)-Based Nanocomposites for Energy Storage Applications. *Phys. Chem. Chem. Phys.* 20 (9), 6598–6605. doi:10.1039/c7cp08312b

Prateek, Thakur, V. K., and Gupta, R. K. (2016). Recent Progress on Ferroelectric Polymer-Based Nanocomposites for High Energy Density Capacitors: Synthesis, Dielectric Properties, and Future Aspects. *Chem. Rev.* 116 (7), 4260–4317. doi:10.1021/acs.chemrev.5b00495

Ren, L., Yang, L., Zhang, S., Li, H., Zhou, Y., Ai, D., et al. (2021). Largely Enhanced Dielectric Properties of Polymer Composites with HfO2 Nanoparticles for High-Temperature Film Capacitors. *Compos. Sci. Technol.* 201, 108528. doi:10.1016/j.compscitech.2020.108528

Ru, J., Min, D., Lanagan, M., Li, S., and Chen, G. (2021). Enhanced Energy Storage Properties of Thermostable Sandwich-Structured BaTiO3/polyimide Nanocomposites with Better Controlled Interfaces. *Mater. Des.* 197, 109270. doi:10.1016/j.matdes.2020.109270

Tang, H., and Sodano, H. A. (2013). Ultra High Energy Density Nanocomposite Capacitors with Fast Discharge Using $Ba_{0.2}Sr_{0.8}TiO_3$ Nanowires. *Nano Lett.* 13 (4), 1373–1379. doi:10.1021/nl3037273

Thakur, Y., Lean, M. H., and Zhang, Q. M. (2017). Reducing Conduction Losses in High Energy Density Polymer Using Nanocomposites. *Appl. Phys. Lett.* 110 (12), 122905. doi:10.1063/1.4979040

Wang, C., He, G., Chen, S., Luo, H., Yang, Y., and Zhang, D. (2022). Achieving High Breakdown Strength and Energy Density in All-Organic Sandwich-Structured Dielectrics by Introducing Polyacrylate Elastomers. *J. Mat. Chem. A* 10, 9103–9113. doi:10.1039/D1TA09933G

Wang, W., Min, D., and Li, S. (2016). Understanding the Conduction and Breakdown Properties of Polyethylene Nanodielectrics: Effect of Deep Traps. *IEEE Trans. Dielect. Electr. Insul.* 23 (1), 564–572. doi:10.1109/TDEI.2015.004823

Wang, Y., Cui, J., Yuan, Q., Niu, Y., Bai, Y., and Wang, H. (2015). Significantly Enhanced Breakdown Strength and Energy Density in Sandwich-Structured Barium Titanate/poly(vinylidene Fluoride) Nanocomposites. *Adv. Mat.* 27 (42), 6658–6663. doi:10.1002/adma.201503186

Wang, Y., Wang, L., Yuan, Q., Niu, Y., Chen, J., Wang, Q., et al. (2017). Ultrahigh Electric Displacement and Energy Density in Gradient Layer-Structured BaTiO3/PVDF Nanocomposites with an Interfacial Barrier Effect. *J. Mat. Chem. A* 5 (22), 10849–10855. doi:10.1039/c7ta01522d

Yu, K., Niu, Y., Zhou, Y., Bai, Y., and Wang, H. (2013). Nanocomposites of Surface-Modified BaTiO3 Nanoparticles Filled Ferroelectric Polymer with Enhanced Energy Density. *J. Am. Ceram. Soc.* 96 (8), 2519–2524. doi:10.1111/jace.12338

Zhang, L., Gao, R., Hu, P., and Dang, Z.-M. (2016). Preparation and Dielectric Properties of Polymer Composites Incorporated with polydopamine@AgNPs Core-Satellite Particles. *RSC Adv.* 6 (41), 34529–34533. doi:10.1039/c6ra00827e

Zhang, X., Jiang, J., Shen, Z., Dan, Z., Li, M., Lin, Y., et al. (2018). Polymer Nanocomposites with Ultrahigh Energy Density and High Discharge Efficiency by Modulating Their Nanostructures in Three Dimensions. *Adv. Mat.* 30 (16), 1707269. doi:10.1002/adma.201707269

Zhang, X., Li, B.-W., Dong, L., Liu, H., Chen, W., Shen, Y., et al. (2018). Superior Energy Storage Performances of Polymer Nanocomposites via Modification of Filler/polymer Interfaces. *Adv. Mat. Interfaces* 5 (11), 1800096. doi:10.1002/admi.201800096

Zheng, M.-S., Zheng, Y.-T., Zha, J.-W., Yang, Y., Han, P., Wen, Y.-Q., et al. (2018). Improved Dielectric, Tensile and Energy Storage Properties of Surface Rubberized BaTiO3/polypropylene Nanocomposites. *Nano Energy* 48, 144–151. doi:10.1016/j.nanoen.2018.03.049

Zhi, X., Mao, Y., Yu, Z., Wen, S., Li, Y., Zhang, L., et al. (2015). γ-Aminopropyl Triethoxysilane Functionalized Graphene Oxide for Composites with High Dielectric Constant and Low Dielectric Loss. *Compos. Part A Appl. Sci. Manuf.* 76, 194–202. doi:10.1016/j.compositesa.2015.05.015

Zhong, S.-L., Dang, Z.-M., and Zha, J.-W. (2018). Prediction on Effective Permittivity of 0-3 Connectivity Particle/polymer Composites at Low Concentration with Finite Element Method. *IEEE Trans. Dielect. Electr. Insul.* 25 (6), 2122–2128. doi:10.1109/TDEI.2018.007193

Zhou, Y., and Wang, Q. (2020). Advanced Polymer Dielectrics for High Temperature Capacitive Energy Storage. *J. Appl. Phys.* 127 (24), 240902. doi:10.1063/5.0009650

Zhou, Y., Yuan, C., Wang, S., Zhu, Y., Cheng, S., Yang, X., et al. (2020). Interface-modulated Nanocomposites Based on Polypropylene for High-Temperature Energy Storage. *Energy Storage Mater.* 28, 255–263. doi:10.1016/j.ensm.2020.03.017

Zhu, Y., Zhu, Y., Huang, X., Chen, J., Li, Q., He, J., et al. (2019). High Energy Density Polymer Dielectrics Interlayered by Assembled Boron Nitride Nanosheets. *Adv. Energy Mat.* 9 (40), 1901826. doi:10.1002/aenm.201901826

Conflict of Interest: The authors declare that the research was conducted in the absence of any commercial or financial relationships that could be construed as a potential conflict of interest.

Publisher's Note: All claims expressed in this article are solely those of the authors and do not necessarily represent those of their affiliated organizations, or those of the publisher, the editors, and the reviewers. Any product that may be evaluated in this article, or claim that may be made by its manufacturer, is not guaranteed or endorsed by the publisher.